RESEARCH ARTICLE

WILEY

A modified fifth-order WENO-Z scheme based on the weights of the reformulated adaptive order WENO scheme

Yize Wang[1,2] | Kunlei Zhao[1,2] | Li Yuan[1,2]

[1]NCMIS & LSEC, Institute of Computational Mathematics and Scientific/Engineering Computing, Academy of Mathematics and Systems Science, Chinese Academy of Sciences, Beijing, People's Republic of China

[2]School of Mathematical Sciences, University of Chinese Academy of Sciences, Beijing, People's Republic of China

Correspondence
Li Yuan, NCMIS & LSEC, Institute of Computational Mathematics and Scientific/Engineering Computing, Academy of Mathematics and Systems Science, Chinese Academy of Sciences, Beijing, 100190, People's Republic of China.
Email: lyuan@lsec.cc.ac.cn

Abstract

A modified fifth-order WENO-Z scheme is proposed by analogy with the non-normalized weights of the reformulated fifth-order adaptive order (AO) WENO scheme. We show that if the original fifth-order WENO-AO scheme is rewritten as the form of the conventional WENO combination, the resulting non-normalized weights can be divided into three parts: a constant one term, a local stencil smoothness measure term and a global stencil smoothness measure term. In order to make use of the latter two terms for constructing a modified WENO-Z scheme with enhanced performance, we change the form of the third term and introduce an adaptive scaling factor to adjust the contributions from the second and third terms. Numerical examples show that the modified fifth-order WENO-Z scheme has the advantage of high resolution in smooth regions and sharp capturing of discontinuities, and it can obtain evidently better results for shocked flows with small-scale structures compared with the recently developed WENO-Z+ and WENO-Z+M schemes.

KEYWORDS

adaptive order, fifth-order accuracy, hyperbolic conservation law, low dissipation, smoothness indicator, WENO scheme

1 | INTRODUCTION

High order schemes capable of capturing strong discontinuities without spurious oscillations and resolving fine-scale structures simultaneously are indispensable for the numerical simulation of complicated supersonic flows. The essentially non-oscillatory (ENO)[1] and weighted ENO (WENO[2]) schemes pioneered developments of many high order shock-capturing schemes in the past four decades. An important advancement is the finite difference WENO-JS schemes developed by Jiang and Shu,[3] in which a smoothness indicator of stencil is defined which can achieve the optimal order of accuracy in smooth monotone regions. The WENO-JS schemes can achieve $(2r-1)$th order of accuracy based on a convex combination of r rth-order ENO stencils for $r = 2$ to $r = 7$.[4] Henrick et al.[5] revealed that the fifth-order WENO-JS scheme may lose accuracy at the first-order critical point where the first derivative of the solution vanishes but not the second and third derivatives, and they derived necessary and sufficient conditions on the weights for fifth-order convergence. By devising a mapping function for the nonlinear weights they developed the WENO-M scheme[5] to retain the optimal order of accuracy at the critical points.[5] Some modified mapping functions were also proposed.[6–8] Borges et al.[9] developed the fifth-order WENO-Z scheme by introducing a reference global smoothness indicator to the calculation of the nonlinear weights, which assign larger weights to discontinuous stencils, resulting in a substantial improvement on numerical resolution of discontinuities. Further, the WENO-Z scheme[9] can achieve fourth-order accuracy at the

first-order critical points whereas the fifth-order WENO-JS scheme[3] can only achieve third-order accuracy and is more dissipative for small-scale flow structures.

Since the WENO-Z schemes have advantages in accuracy, resolution, shock-capturing, and overall efficiency,[10,11] many newly developed WENO schemes adopt the WENO-Z type weights, such as WENO-NS,[12] P-WENO,[13] MR-WENO,[14] adaptively central-upwind WENO schemes,[15,16] WENO-MS,[17] to name a few. It has been recognized that the key to high resolution is to let the nonlinear weights approach the ideal weights in smooth regions as quickly as possible so that the scheme can approach the underlying linear scheme better.[9] More recently, by adding a new term to the non-normalized weights of the original WENO-Z scheme, Acker et al.[18] developed the fifth-order WENO-Z+ scheme. This new term is used to increase the weights of less smooth substencils which are always smaller than the corresponding ideal weights. The WENO-Z+ scheme can attain better resolution in smooth regions of the solution for some benchmark problems while having the same numerical stability of the original WENO-Z scheme, however, it achieves little improvement over the original WENO-Z scheme for complex problems having multi-scale structures. Later, Luo and Wu[19] proposed the WENO-Z+M scheme (M means modified). With a modified form for the new term, the WENO-Z+M scheme assigns a larger weight to the less smooth substencil, thus achieving spectral properties and accuracy superior to the WENO-Z+ scheme. However, the new term in the WENO-Z+ or WENO-Z+M scheme contains a mesh size Δx dependent factor, which makes the scheme lose the scale-invariant property.[20]

Unlike the classical finite difference WENO schemes which adopt the combination of several equal-sized small stencils, the central WENO (CWENO) schemes as developed by Levy et al.[21,22] adopt the combination of a large central stencil and several small stencils, in which the underlying linear weights can be any positive and symmetric numbers with only the requirement that their sum equals one. With this combination strategy, Capdeville[23] developed a fifth-order central WENO finite volume scheme for the Euler equations on 1D non-uniform meshes, and Cravero and Semplice[24] developed third-order CWENO schemes on 1D and 2D non-uniform meshes. Cravero et al.[25] generalized the CWENO reconstructions up to 9th order with the WENO-JS nonlinear weights. Using a similar combination strategy, Zhu and Qiu[26] developed a fifth-order finite difference WENO-Z-weights scheme, in which the underlying linear weights can be any positive numbers (not necessarily symmetric) with only the requirement that their sum equals one and thus one can reduce numerical dissipation by choosing suitable linear weights, and the combination procedure can be easily extended to finite volume methods on unstructured grids without the plague of negative ideal weights.[27,28] Balsara et al.[29] generalized the work[26] to 7th and 9th orders by recursively making the combination of a high-order (WENO) reconstruction and a(several) low-order (WENO) reconstruction(s) and called the resulting schemes as WENO-AO (adaptive order) schemes. The WENO-AO schemes were extended to unstructured grids.[30] However, the shortcoming of the AO weighting strategy is the larger computational cost and possible oscillations due to inappropriate choice of the linear weights.

In this article, we first connect the fifth-order WENO-AO scheme[29] with the original WENO-Z scheme.[9] We reformulate the WENO-AO scheme[29] as the conventional WENO convex combination form, and show that there are three terms in the resulting non-normalized weights: the first two terms are similar to those in the original WENO-Z weights, and the third term is associated with the five-point global stencil smoothness indicator and is similar to the new term in the WENO-Z+[18] or WENO-Z+M scheme.[19] Then, we modify the original WENO-Z scheme by analogy with the non-normalized WENO-AO weights. We let the scaling factor in the last two terms vary with the smoothness of the five-point global stencil, and modify the third term to reduce computational cost and increase the weights of less smooth substencils. The performance of the modified WENO-Z scheme (named as WENO-MZ) is demonstrated in a series of numerical examples by comparison with the fifth-order WENO-JS, WENO-Z, WENO-Z+, WENO-Z+M and WENO-AO schemes. The results show that the new scheme always has better resolution than the other schemes and its computational cost is only a bit more than that of the WENO-Z+M scheme.

The remainder of this article proceeds as follows. In Section 2, we give a brief review of the fifth-order WENO-JS, WENO-Z and WENO-AO schemes relevant to this study. In Section 3, the WENO-AO scheme is rewritten as a WENO-Z like scheme, and based on the compositional terms of the non-normalized weights, the modified WENO-Z scheme is proposed. In Section 4 numerical results of one- and two-dimensional (1D and 2D) benchmark problems are presented to show the performance of the present WENO-MZ scheme. Concluding remarks are given in Section 5.

2 | REVIEW OF THE FIFTH-ORDER WENO SCHEMES

Consider the one-dimensional scalar hyperbolic conservation law

$$u_t(x,t) + f(u(x,t))_x = 0, \tag{1}$$

where u is the sought solution, and f is the flux function. The computational domain $x \in [a, b]$ is divided into N non-overlapping cells $I_i = [x_{i-1/2}, x_{i+1/2}]$ with the cell center $x_i = (x_{i-1/2} + x_{i+1/2})/2$. Without loss of generality, we shall use only uniform cells, and the cell size is $\Delta x = x_{i+1/2} - x_{i-1/2}$. Using a conservative finite difference scheme, the semi-discretized form of Equation (1) can be written as

$$\frac{\mathrm{d}u_i}{\mathrm{d}t} = -\frac{1}{\Delta x}\left(\hat{f}_{i+1/2} - \hat{f}_{i-1/2}\right) := L(u), \tag{2}$$

where the numerical flux $\hat{f}_{i+1/2} = \hat{f}_{i+1/2}^+ + \hat{f}_{i+1/2}^-$, and $\hat{f}_{i+1/2}^+$ and $\hat{f}_{i+1/2}^-$ denote the numerical fluxes for the split positive and negative fluxes f^+ and f^-, which satisfy $f = f^+ + f^-$. In this work, the semi-discrete system of ordinary differential equations (2) is solved by using the third-order strong stability-preserving Runge–Kutta method[31]:

$$\begin{cases} u^{(1)} = u^n + \Delta t L(u^n), \\ u^{(2)} = \frac{3}{4}u^n + \frac{1}{4}\left(u^{(1)} + \Delta t L(u^{(1)})\right), \\ u^{n+1} = \frac{1}{3}u^n + \frac{2}{3}\left(u^{(2)} + \Delta t L(u^{(2)})\right). \end{cases} \tag{3}$$

Hereafter, we restrict our attention to the reconstruction of the numerical flux $\hat{f}_{i+1/2}$. Due to the symmetry, only the positive flux $\hat{f}_{i+1/2}^+$ is described and the superscript "+" on the positive fluxes is omitted for brevity.

2.1 | WENO-JS and WENO-Z schemes

The fifth-order WENO flux is reconstructed on a five-point global stencil $S_5 = \{x_{i-2}, x_{i-1}, x_i, x_{i+1}, x_{i+2}\}$ by the weighted average of the three third-order numerical fluxes, $\hat{f}_{i+1/2}^k$, reconstructed on the three substencils, $S_k = \{x_{i-2+k}, x_{i-1+k}, x_{i+k}\}$, $k = 0, 1, 2$:

$$\begin{aligned} \hat{f}_{i+1/2}^0 &= \frac{1}{3}f_{i-2} - \frac{7}{6}f_{i-1} + \frac{11}{6}f_i, \\ \hat{f}_{i+1/2}^1 &= -\frac{1}{6}f_{i-1} + \frac{5}{6}f_i + \frac{1}{3}f_{i+1}, \\ \hat{f}_{i+1/2}^2 &= \frac{1}{3}f_i + \frac{5}{6}f_{i+1} - \frac{1}{6}f_{i+2}. \end{aligned} \tag{4}$$

Through the convex combination of the low order numerical fluxes, $\hat{f}_{i+1/2}^k$, $k = 0, 1, 2$, one can build a fifth-order WENO numerical flux as the following:

$$\hat{f}_{i+1/2} = \sum_{k=0}^{2} \omega_k \hat{f}_{i+1/2}^k, \tag{5}$$

where ω_k is the nonlinear weights. For calculating these weights, the local smoothness indicators of substencil β_k are determined using the formula given by Jiang and Shu[3]

$$\beta_k = \sum_{l=1}^{2} \int_{x_{i-1/2}}^{x_{i+1/2}} \Delta x^{2l-1}\left(\frac{\mathrm{d}^l P_k(x)}{\mathrm{d}x^l}\right)^2 \mathrm{d}x, \quad k = 0, 1, 2, \tag{6}$$

where $P_k(x)$ are the reconstruction polynomials on the substencils. The detailed local smoothness indicators are given by[3]

$$\begin{cases} \beta_0 = \frac{1}{4}(f_{i-2} - 4f_{i-1} + 3f_i)^2 + \frac{13}{12}(f_{i-2} - 2f_{i-1} + f_i)^2, \\ \beta_1 = \frac{1}{4}(f_{i-1} - f_{i+1})^2 + \frac{13}{12}(f_{i-1} - 2f_i + f_{i+1})^2, \\ \beta_2 = \frac{1}{4}(3f_i - 4f_{i+1} + f_{i+2})^2 + \frac{13}{12}(f_i - 2f_{i+1} + f_{i+2})^2. \end{cases} \tag{7}$$

With Equation (7), the nonlinear weights for the 5th-order WENO-JS[3] and WENO-Z[9] schemes are given by

$$
\omega_k = \frac{\alpha_k}{\sum_{l=0}^{2} \alpha_l}, \quad \alpha_k = \frac{\gamma_k}{(\beta_k + \epsilon)^2}, \quad \text{(WENO-JS)},
$$
$$
\omega_k = \frac{\alpha_k}{\sum_{l=0}^{2} \alpha_l}, \quad \alpha_k = \gamma_k \left(1 + \left(\frac{\tau_5}{\beta_k + \epsilon} \right)^q \right), \quad \text{(WENO-Z)}.
$$
(8)

Here, the ideal weights are $\{\gamma_0, \gamma_1, \gamma_2\} = \left\{ \frac{1}{10}, \frac{6}{10}, \frac{3}{10} \right\}$, and we take $\epsilon = 10^{-6}$ for the WENO-JS scheme and $\epsilon = 10^{-40}$ for the WENO-Z scheme to avoid division by zero. For the WENO-Z scheme, the reference global smoothness indicator $\tau_5 = |\beta_0 - \beta_2| \sim \mathcal{O}(\Delta x^5)$, and the power q takes 1 or 2 ($q = 1$ gives less dissipation near discontinuities than $q = 2$, but $q = 2$ can keep the optimal order of accuracy at the first-order critical points).

2.2 | WENO-AO scheme

From the previous WENO reconstruction process, it can be seen that by increasing the number of substencils and grid points per substencil, higher order WENO schemes can be obtained, and in general, higher order schemes have smaller numerical dissipation. However, increasing the number of grid points in substencils increases the probability containing discontinuities. Although higher order WENO scheme can automatically adjust the weights of substencils, they may have poor numerical performance when computing complex problems. In addition, when the WENO-JS class methods are extended to unstructured grids, there will be the issue of negative ideal weights. In contrast, the WENO-AO schemes[26,29] use another strategy to combine the reconstruction polynomials and are free of the issue. The process is as follows:

1. Select a set of substencils and corresponding linear weights $\{d_k\}$, as well as the global stencil and corresponding linear weight d_h. The weight value can be any positive number as long as the sum of all the linear weights is equal to 1. This is different from the ideal weights of the WENO-JS class methods.
2. Reconstruct the high order polynomial p_h on the global stencil and lower order polynomials $\{p_k\}$ on the set of substencils. Calculate $\hat{p}_h = p_h - \sum_k d_k p_k$.
3. Calculate the nonlinear weights $\{\omega_k\}$ of substencils and the nonlinear weight ω_h of the global stencil.
4. Get the final numerical flux by the weighted combination, $\hat{f} = \frac{\omega_h}{d_h} \hat{p}_h + \sum_k \omega_k p_k$.

The fifth-order WENO-AO scheme with three substencils, called WENO-AO(5,3),[29] has the same global stencil S_5 and three substencils S_0, S_1, S_2 as the fifth-order WENO-JS scheme.[3] The linear weights d_h, d_0, d_1, d_2 are chosen as follows[29]:

$$
d_h = \gamma_H, \quad d_0 = d_2 = (1 - \gamma_H) \frac{(1 - \gamma_L)}{2}, \quad d_1 = (1 - \gamma_H) \gamma_L,
$$
(9)

where $\gamma_H, \gamma_L \in [0.85, 0.95]$, and in this article we take $\gamma_H = \gamma_L = 0.85$, thus $\{d_0, d_1, d_2, d_h\} = \{0.01125, 0.1275, 0.01125, 0.85\}$.

The global smoothness indicator $\beta_h = \beta_5$ for the five-point global stencil is calculated according to the formula[29] similar to Equation (6) as follows

$$
\beta_h = \beta_5 = \left(u_x + \frac{u_{x3}}{10} \right)^2 + \frac{13}{3} \left(u_{x2} + \frac{123}{455} u_{x4} \right)^2 + \frac{781}{20} (u_{x3})^2 + \frac{14211461}{2275} (u_{x4})^2.
$$
(10)

Here, the coefficients are given as[29]

$$
\begin{aligned}
u_x &= \frac{1}{120} (11 f_{i-2} - 82 f_{i-1} + 82 f_{i+1} - 11 f_{i+2}), \\
u_{x2} &= \frac{1}{56} (-3 f_{i-2} + 40 f_{i-1} - 74 f_i + 40 f_{i+1} - 3 f_{i+2}), \\
u_{x3} &= \frac{1}{12} (-f_{i-2} + 2 f_{i-1} - 2 f_{i+1} + f_{i+2}), \\
u_{x4} &= \frac{1}{24} (f_{i-2} - 4 f_{i-1} + 6 f_i - 4 f_{i+1} + f_{i+2}).
\end{aligned}
$$
(11)

Like the WENO-Z schemes, a reference global smoothness indicator is defined as

$$\tau = \frac{|\beta_h - \beta_0| + |\beta_h - \beta_1| + |\beta_h - \beta_2|}{3},$$ (12)

where β_0, β_1 and β_2 are the same as Equation (7). Then, the nonlinear weights of the WENO-AO(5,3) scheme are defined as

$$\omega_k = \frac{\alpha_k}{\alpha_0 + \alpha_1 + \alpha_2 + \alpha_h}, k = 0, 1, 2, h, \quad \alpha_k = d_k \left[1 + \left(\frac{\tau}{\beta_k + \epsilon} \right)^q \right], \quad k = 0, 1, 2, h,$$ (13)

where $\epsilon = 10^{-40}$, and the power q is usually taken as 2 to avoid numerical oscillations near discontinuities.

In the end we get the numerical flux of the WENO-AO(5,3) scheme as

$$\hat{f}_{i+1/2}^{AO(5,3)} = \frac{\omega_h}{d_h}(p_h - d_0 p_0 - d_1 p_1 - d_2 p_2) + \omega_0 p_0 + \omega_1 p_1 + \omega_2 p_2,$$ (14)

where the three low order fluxes p_k, $k = 0, 1, 2$, are the same as Equation (4), and the high order (fifth-order) flux p_h is given by

$$p_h = \frac{1}{60}(2f_{i-2} - 13f_{i-1} + 47f_i + 27f_{i+1} - 3f_{i+2}).$$ (15)

3 | MODIFIED WENO-Z SCHEME

From the review in Section 2 we can see that the WENO-AO scheme is different from the conventional WENO combination and it is hard to discover their similarity. However, we have found that for some numerical examples the WENO-AO(5,3) scheme[29] exhibits a very consistent numerical performance with the WENO-Z5 scheme,[9] which may imply some potential connection between them. Hu[32] first explored this connection by reformulating the WENO-Z5 scheme as a combination of a 5-points global stencil and three 3-points substencils like the WENO-AO(5,3) scheme. In this section, we will rewrite the WENO-AO(5,3) scheme as the conventional WENO combination form and reveal the relationship between the two schemes, and then propose a modified WENO-Z scheme based on this relationship.

Rewrite Equation (14) as

$$\hat{f}_{i+1/2}^{AO} = \frac{\omega_h}{d_h}(p_h - d_0 p_0 - d_1 p_1 - d_2 p_2) + \omega_0 p_0 + \omega_1 p_1 + \omega_2 p_2.$$ (16)

Denote the ideal weights $\{\gamma_0, \gamma_1, \gamma_2\} = \{0.1, 0.6, 0.3\}$. Then we have

$$p_h = \gamma_0 p_0 + \gamma_1 p_1 + \gamma_2 p_2.$$ (17)

Inserting Equation (17) into Equation (16) we can get

$$\hat{f}_{i+1/2}^{AO} = \left(\frac{\omega_h(\gamma_0 - d_0)}{d_h} + \omega_0 \right) p_0 + \left(\frac{\omega_h(\gamma_1 - d_1)}{d_h} + \omega_1 \right) p_1 + \left(\frac{\omega_h(\gamma_2 - d_2)}{d_h} + \omega_2 \right) p_2.$$ (18)

Define the combination coefficients before the low order fluxes p_k as χ_k:

$$\chi_k = \omega_k + \frac{\omega_h}{d_h}(\gamma_k - d_k), \quad k = 0, 1, 2.$$ (19)

Substituting the original WENO-AO(5,3) weights (13) into Equation (19), we obtain

$$\chi_k = d_k \frac{\left(1 + \left(\frac{\tau}{\beta_k + \epsilon} \right)^q \right)}{\alpha_0 + \alpha_1 + \alpha_2 + \alpha_h} + \frac{\left(1 + \left(\frac{\tau}{\beta_h + \epsilon} \right)^q \right)}{\alpha_0 + \alpha_1 + \alpha_2 + \alpha_h}(\gamma_k - d_k), \quad k = 0, 1, 2.$$ (20)

The denominator part in Equation (20) is not related to k, so we only need to analyze the numerator part. Use $\hat{\chi}_k$ to represent the numerator part, which is given by

$$\hat{\chi}_k = \gamma_k \left[1 + \frac{d_k}{\gamma_k} \left(\frac{\tau}{\beta_k + \epsilon} \right)^q + \left(1 - \frac{d_k}{\gamma_k} \right) \left(\frac{\tau}{\beta_h + \epsilon} \right)^q \right], \quad k = 0, 1, 2. \tag{21}$$

Comparing Equation (21) with the corresponding non-normalized weights α_k in the second row of Equation (8), we find that the weights of the reformulated WENO-AO(5,3) scheme are similar to the WENO-Z weights. Equation (21) consists of three parts:

1. A linear part (constant 1.0). It serves as two purposes: first, it serves as a reference value for stencil smoothness measurements; second, it serves as a condition for the scheme to achieve the optimal order of accuracy.
2. A local smoothness measurement part $(d_k/\gamma_k)(\tau/(\beta_k + \epsilon))^q$. The coefficient d_k/γ_k acts as a scaling factor for the same term as in the original WENO-Z scheme. According to the choice (9), the linear weights $\{d_0, d_1, d_2\} = \{0.01125, 0.1275, 0.01125\}$ are smaller than the corresponding ideal weights $\{\gamma_0, \gamma_1, \gamma_2\} = \{0.1, 0.6, 0.3\}$, and thus this part is smaller than the term in the original WENO-Z scheme. In smooth regions of the solution, this can make the WENO-AO(5,3) scheme more resemble the fifth-order linear upwind scheme. However, in non-smooth regions of the solution, this may cause numerical oscillations. This is the reason why the WENO-AO(5,3) scheme often chooses $q = 2$ to increase dissipation near discontinuities for numerical stability rather than $q = 1$.
3. An additional term associated with the five-point global stencil smoothness indicator β_h and scaled by the coefficient $(1 - d_k/\gamma_k)$. It looks like the additional correction term in the WENO-Z+[18] or WENO-Z+M[19] scheme. Its role is to increase the weight of less smooth substencils and improve resolution near discontinuities.

From the above analysis, it is seen that the WENO-AO(5,3) scheme is essentially a modification to the WENO-Z scheme. Our numerical experiment indicates that with the choice of the linear weights (9), the WENO-AO(5,3) scheme performs better in smooth regions but worse in non-smooth regions than the WENO-Z scheme. In this article, we develop a new variant of WENO-Z scheme by modifying the non-normalized weights (21). First, we replace the fixed scaling factor d_k/γ_k by an adaptive one that can quickly approach 0 in smooth regions to make the scheme close to the linear upwind scheme, and quickly approach 1 near discontinuities to make the scheme close to the WENO-Z scheme. Second, we change τ and β_h in (21).

By replacing d_k/γ_k with an adaptive scaling factor $\eta \in [0, 1]$ and τ with $\tau_5 = |\beta_0 - \beta_2|$ in (21), we can define the non-normalized weights for a modified fifth-order WENO-Z scheme as

$$\alpha_k^{\text{MZ}'} = \gamma_k \left[1 + \eta \left(\frac{\tau_5}{\beta_k + \epsilon} \right)^q + (1 - \eta) \left(\frac{\tau_5}{\beta_h + \epsilon} \right)^q \right], \quad k = 0, 1, 2. \tag{22}$$

After some experience, we design η as

$$\eta = \left[\frac{|\beta_0 - \beta_2|}{\max(\beta_0, \beta_2) + \epsilon} \right]^4. \tag{23}$$

As the computational cost for calculating β_h using Equation (10) is high, we simply use $\beta_h = \max_{0 \leq k \leq 2}\{\beta_k\}$ in (22) initially. However, our numerical experiment[33] shown that this choice of β_h gains little improvement in resolution over the original WENO-Z scheme. The reason may be that the third term in (22) is a less-than-one constant for all the substencils S_k, $k = 0, 1, 2$.

In the following, we design a new β_h for (22), which can increase the magnitude of the third term differently for different substencils. For this goal, we make use of the local smoothness indicator $\hat{\beta}_1$[34,35] for the substencil $S_1 = \{x_{i-1}, x_i, x_{i+1}\}$ which is based on all the derivatives of the Lagrange interpolation polynomial on S_1 evaluated at the center x_i of the big stencil S_5,

$$\hat{\beta}_1 = \frac{1}{4}(f_{i-1} - f_{i+1})^2 + (f_{i-1} - 2f_i + f_{i+1})^2. \tag{24}$$

Using the Taylor series expansion at the point x_i, β_1 in Equation (7) and $\hat{\beta}_1$ in Equation (24) can be written as

$$
\begin{aligned}
\beta_1 &= \left(f_i' \Delta x\right)^2 + \left(\frac{13}{12} f_i''^2 + \frac{1}{3} f_i' f_i'''\right) \Delta x^4 + \mathcal{O}(\Delta x^6), \\
\hat{\beta}_1 &= \left(f_i' \Delta x\right)^2 + \left(f_i''^2 + \frac{1}{3} f_i' f_i'''\right) \Delta x^4 + \mathcal{O}(\Delta x^6).
\end{aligned}
\tag{25}
$$

From Equation (25) we can construct a new smoothness measurement B_4 as

$$
B_4 = \left|\beta_1 - \hat{\beta}_1\right| = \frac{1}{12}(f_{i-1} - 2f_i + f_{i+1})^2, \ \sim \mathcal{O}(\Delta x^4),
\tag{26}
$$

which is smaller than $\beta_h \sim \mathcal{O}(\Delta x^2)$ (Equation 10) in magnitude in smooth regions. Furthermore, we design a new $\beta_h = t_k B_4$ for use in Equation (22), where t_k is a substencil-dependent coefficient defined as:

$$
t_0 = \frac{|\beta_0 - \beta_1| + |\beta_2 - \beta_1| + 2\epsilon}{|\beta_0 - \beta_1| + \epsilon} = 1 + r, \quad t_1 \equiv 2, \quad t_2 = \frac{|\beta_0 - \beta_1| + |\beta_2 - \beta_1| + 2\epsilon}{|\beta_2 - \beta_1| + \epsilon} = 1 + \frac{1}{r}, \quad \text{where } r = \frac{|\beta_2 - \beta_1| + \epsilon}{|\beta_0 - \beta_1| + \epsilon}.
\tag{27}
$$

Finally, we define the non-normalized weights for the present modified WENO-Z scheme as follows,

$$
\alpha_k^{\mathrm{MZ}} = \gamma_k \left[1 + \eta \left(\frac{\tau_5}{\beta_k + \epsilon}\right)^q + (1 - \eta)\left(\frac{\tau_5}{t_k B_4 + \epsilon}\right)^q\right], \quad k = 0, 1, 2.
\tag{28}
$$

The ideal weights γ_k, reference global smoothness indicator τ_5 and small parameter $\epsilon = 10^{-40}$ are completely the same as those of the original fifth-order WENO-Z scheme. We take $q = 1$ in Equation (28).

In smooth regions of the solution, τ_5 has the order of $\mathcal{O}(\Delta x^5)$, $t_k B_4$ has the order of $\mathcal{O}(\Delta x^4)$, the three coefficients t_k are close to each other ($t_k \approx 2, \forall k = 0, 1, 2$), and η is small, so the third term in Equation (28) almost becomes a larger constant. This means that the first and third terms dominate α_k^{MZ} in smooth regions so as to make the scheme approach the fifth-order linear upwind scheme better. Near discontinuities, t_k can be quite different for different substencils. For example, if β_0 is the largest (meaning that the substencil S_0 is less smooth than S_1 and S_2), then $r < 1$ and thus t_0 will be less than 2 and even close to 1. Now we have $t_0 < t_1 < t_2$ and this will amplify the third term in (28) for the less smooth substencil S_0, which will improve resolution near discontinuities.[9,18] However, this amplification is controlled automatically since the coefficient $(1 - \eta)$ in the third term also becomes small near discontinuities as per Equation (23), thus avoiding numerical oscillations and instability.

We name the modified fifth-order scheme as WENO-MZ, where M stands for "modified." As comparison, we list the non-normalized weights α_k of the WENO-Z+[18] and WENO-Z+M[19] schemes respectively as follows:

1. WENO-Z+: $\alpha_k = \gamma_k \left[1 + \left(\frac{\tau_5 + \epsilon}{\beta_k + \epsilon}\right)^q + \Delta x^{2/3}\left(\frac{\beta_k + \epsilon}{\tau_5 + \epsilon}\right)\right], \quad k = 0, 1, 2;$

2. WENO-Z+M: $\alpha_k = \gamma_k \left[1 + (\xi_k)^q + \Delta x^{2/3} \frac{1 + \xi_{\min}^2}{\sum_{l=0}^2 \gamma_l (1 + \xi_l^2)}\left(\frac{1}{\xi_k}\right)^{1/2}\right], \quad \xi_k = \frac{\tau_5 + \epsilon}{\beta_k + \epsilon}, \quad \xi_{\min} = \min_{0 \le k \le 2}(\xi_k), \quad k = 0, 1, 2.$

Finally, the normalized weights for all the WENO-Z type schemes are as usual: $\omega_k = \alpha_k / \sum_{l=0}^2 \alpha_l, \ k = 0, 1, 2$.

4 | NUMERICAL RESULTS

In this section, we provide some numerical tests in 1D and 2D problems to demonstrate the performance of the proposed WENO-MZ scheme in comparison with the 5th-order WENO-JS, WENO-AO, WENO-Z, WENO-Z+ and WENO-Z+M schemes. For fair comparison we take the same index $q = 1$ for the WENO-MZ, WENO-Z, WENO-Z+ and WENO-Z+M schemes. Since the WENO-AO scheme with $q = 1$ diverges in calculating the double Mach reflection problem we always use $q = 2$ as per the Reference 29. And we use $\epsilon = 10^{-40}$ for all the WENO schemes except $\epsilon = 10^{-6}$ for the WENO-JS scheme. The third-order TVD Runge–Kutta method[31] is used for time stepping. CFL number is set to 0.5 for all cases. As we find that the accuracy and resolution of the WENO-AO scheme are between the WENO-Z and WENO-Z+M schemes while it has larger computational cost than all other schemes, we will compare the WENO-AO scheme with other schemes only in two-dimensional examples.

4.1 | Accuracy test

The accuracy test is carried out for the two-dimensional vortex evolution problem for the Euler equations.[27,36] The compressible Euler equations of gas dynamics are given as

$$\mathbf{U}_t + \mathbf{F}(\mathbf{U})_x + \mathbf{G}(\mathbf{U})_y = 0, \tag{29}$$

where the solution vector and flux vectors are given by

$$\mathbf{U} = (\rho, \rho u, \rho v, E)^T, \quad \mathbf{F}(\mathbf{U}) = \left(\rho u, \rho u^2 + p, \rho uv, u(E + p)\right)^T, \quad \mathbf{G}(\mathbf{U}) = \left(\rho v, \rho uv, \rho v^2 + p, v(E + p)\right)^T.$$

Here ρ is the density, (u, v) is the velocity, E is the total energy, p is the pressure and the equation of state is

$$E = \frac{p}{\gamma - 1} + \frac{1}{2}\rho(u^2 + v^2), \quad \gamma = 1.4.$$

The mean flow is $\rho = 1, p = 1$ and $(u, v) = (1, 1)$. At the time $t = 0$, we add, to the mean flow, an isentropic vortex (perturbations in u, v and the temperature $T = p/\rho$, no perturbation in the entropy $S = p/\rho^\gamma$)

$$
\begin{aligned}
(\delta u, \delta v) &= \frac{\varepsilon}{2\pi} e^{0.5(1-r^2)}(-\bar{y}, \bar{x}), \\
\delta T &= -\frac{(\gamma - 1)\varepsilon^2}{8\gamma\pi^2} e^{1-r^2}, \\
\delta S &= 0,
\end{aligned}
\tag{30}
$$

with $(\bar{x}, \bar{y}) = (x - 5, y - 5), r^2 = \bar{x}^2 + \bar{y}^2$ and the vortex strength $\varepsilon = 5$. The computational domain is taken as $[0, 10] \times [0, 10]$, and periodic boundary conditions are used in both directions. It is clear that the exact solution of Equation (29) with the above initial and boundary conditions is just the passive convection of the vortex with the mean velocity.

The 2D Euler equations are solved with the finite difference WENO schemes in the dimension-by-dimension fashion. In each dimension the WENO reconstructions are performed in the characteristic fields. The global Lax-Friedrichs (GLF) flux splitting with different maximum eigenvalues for different characteristic fields taken over a grid line[36,37] is used if not mentioned otherwise. The time step is calculated with the following formula:

$$\Delta t = \text{CFL}\frac{\Delta t_x \Delta t_y}{\Delta t_x + \Delta t_y}, \quad \Delta t_x = \frac{\Delta x}{\max\limits_{\forall i,j}(|u_{i,j}| + c_{i,j})}, \quad \Delta t_y = \frac{\Delta y}{\max\limits_{\forall i,j}(|v_{i,j}| + c_{i,j})}, \quad c_{i,j} = \sqrt{\gamma\frac{p_{i,j}}{\rho_{i,j}}}.$$

We first compute the solutions of various schemes to $t = 2.0$ for the accuracy test. The accuracy results are shown in Table 1 for uniform meshes with $N_x = N_y$ refined in both directions. Both the L_1 and L_∞ errors presented are for the point values of ρ,

$$
\begin{aligned}
L_1 &= \frac{L_x L_y}{N_x N_y}\sum_{i=1}^{N_x}\sum_{j=1}^{N_y}\left|\rho_{i,j} - \rho_{i,j}^{\text{exact}}\right|, \\
L_\infty &= \max_{\forall i,j}\left|\rho_{i,j} - \rho_{i,j}^{\text{exact}}\right|.
\end{aligned}
$$

From Table 1 we see that the errors of the WENO-JS scheme are the largest, and the errors descend in the sequence of the WENO-Z+, WENO-Z, WENO-Z+M and WENO-MZ schemes. Notice that the WENO-Z+M and WENO-MZ results are very close. The numerical orders of accuracy are comparable to the theoretical ones.

TABLE 1 Accuracy for the 2D Euler equations for the smooth vortex evolution problem (30), $t = 2.0$.

Mesh	WENO-JS		WENO-Z		WENO-Z+		WENO-Z+M		WENO-MZ	
	L_1	Order	L_1	Order	L_1	Order	L_1	Order	L_1	Order
20	1.95E−3	–	5.15E−4	–	6.03E−4	–	3.93E−4	–	4.12E−4	–
40	1.57E−4	3.63	4.05E−5	3.67	4.70E−5	3.68	3.15E−5	3.64	3.60E−5	3.52
80	7.24E−6	4.44	3.28E−6	3.63	6.07E−6	2.95	2.78E−6	3.50	2.01E−6	4.16
160	2.55E−7	4.83	8.08E−8	5.34	1.75E−7	5.12	6.36E−8	5.45	7.76E−8	4.69
320	9.67E−9	4.72	2.81E−9	4.85	5.24E−9	5.06	2.74E−9	4.54	2.69E−9	4.85
Mesh	L_∞	Order	L_∞	Order	L_∞	Order	L_∞	Order	L_∞	Order
20	5.46E−3	–	1.53E−3	–	1.58E−3	–	1.24E−3	–	1.09E−3	–
40	4.99E−4	3.45	1.03E−4	3.89	1.61E−4	3.29	8.67E−5	3.84	9.57E−5	3.51
80	2.86E−5	4.12	1.39E−5	2.89	2.00E−5	3.01	1.00E−5	3.12	1.00E−5	3.26
160	8.67E−7	5.04	3.89E−7	5.16	7.42E−7	4.75	3.14E−7	4.99	3.61E−7	4.79
320	3.16E−8	4.78	8.80E−9	5.47	1.86E−8	5.32	9.84E−9	5.00	8.53E−9	5.40
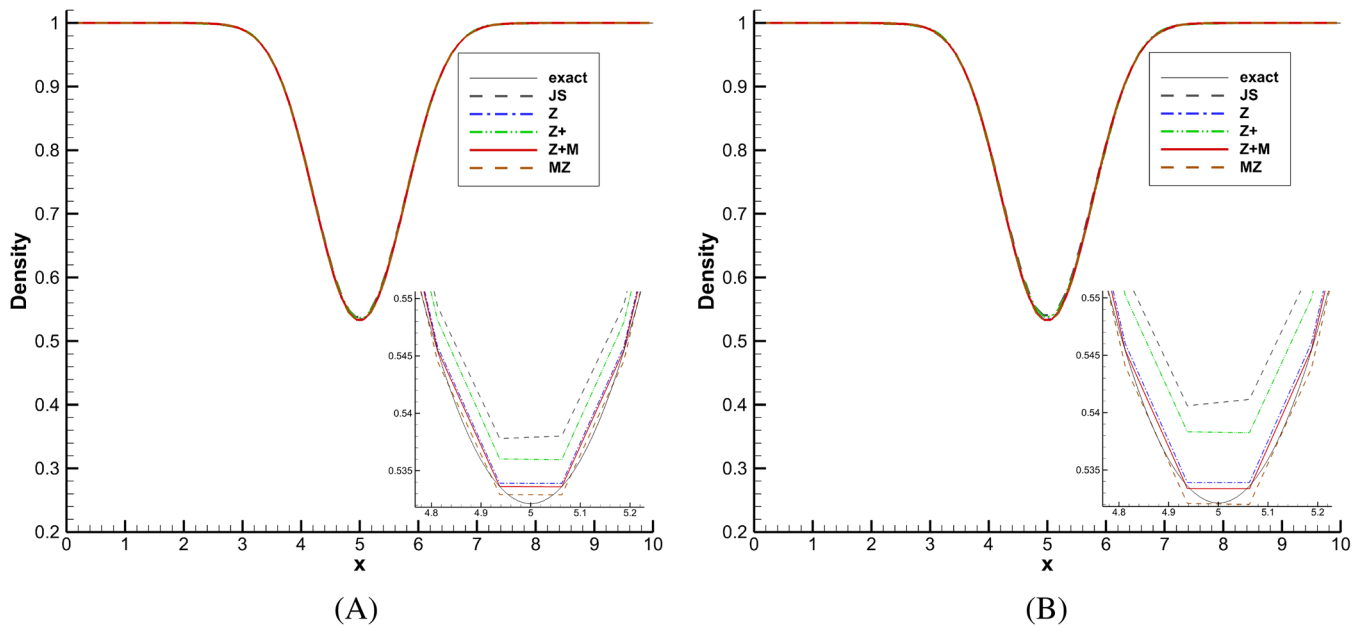
FIGURE 1 Density profiles at $y = 5$ and two instants for the 2D vortex evolution, $N_x = N_y = 80$. (A) $t = 50$ (B) $t = 100$. [Colour figure can be viewed at wileyonlinelibrary.com]

We then fix the mesh at $N_x = N_y = 80$ and compute the long-time evolution of the vortex. Figure 1 shows the result comparison among the different schemes at $t = 50$ and 100. We show the line cut through the center of the vortex for the density ρ. It is easy to see the present WENO-MZ result is better than the WENO-Z+M result.

4.2 | Linear advection equation

Second, we consider a non-smooth solution of the linear advection equation:

$$u_t + u_x = 0, \quad -1 \le x \le 1, \quad t > 0. \tag{31}$$

The initial condition as given by Jiang and Shu[3] contains a Gaussian, a square-wave, a triangle and a semi-ellipse wave with periodical boundary conditions

$$u(x,0) = \begin{cases} \frac{1}{6}[G(x,\beta,z-\delta) + 4G(x,\beta,z) + G(x,\beta,z+\delta)], & x \in [-0.8,-0.6], \\ 1, & x \in [-0.4,-0.2], \\ 1 - |10(x-0.1)|, & x \in [0,0.2], \\ \frac{1}{6}[F(x,\alpha,a-\delta) + 4F(x,\alpha,a) + F(x,\alpha,a+\delta)], & x \in [0.4,0.6], \\ 0, & \text{elsewhere}, \end{cases} \tag{32}$$

where $G(x,\beta,z) = e^{-\beta(x-z)^2}, F(x,\alpha,a) = \sqrt{\max(1-\alpha^2(x-a)^2,0)}, z = -0.7, \delta = 0.005, \beta = \log 2/36\delta^2, a = 0.5, \alpha = 10$.

Figure 2 shows comparison of the numerical results at the final time $t = 6$. We can see that the results by the present WENO-MZ, WENO-Z, WENO-Z+, and WENO-Z+M schemes are nearly same and are all better than the WENO-JS result.
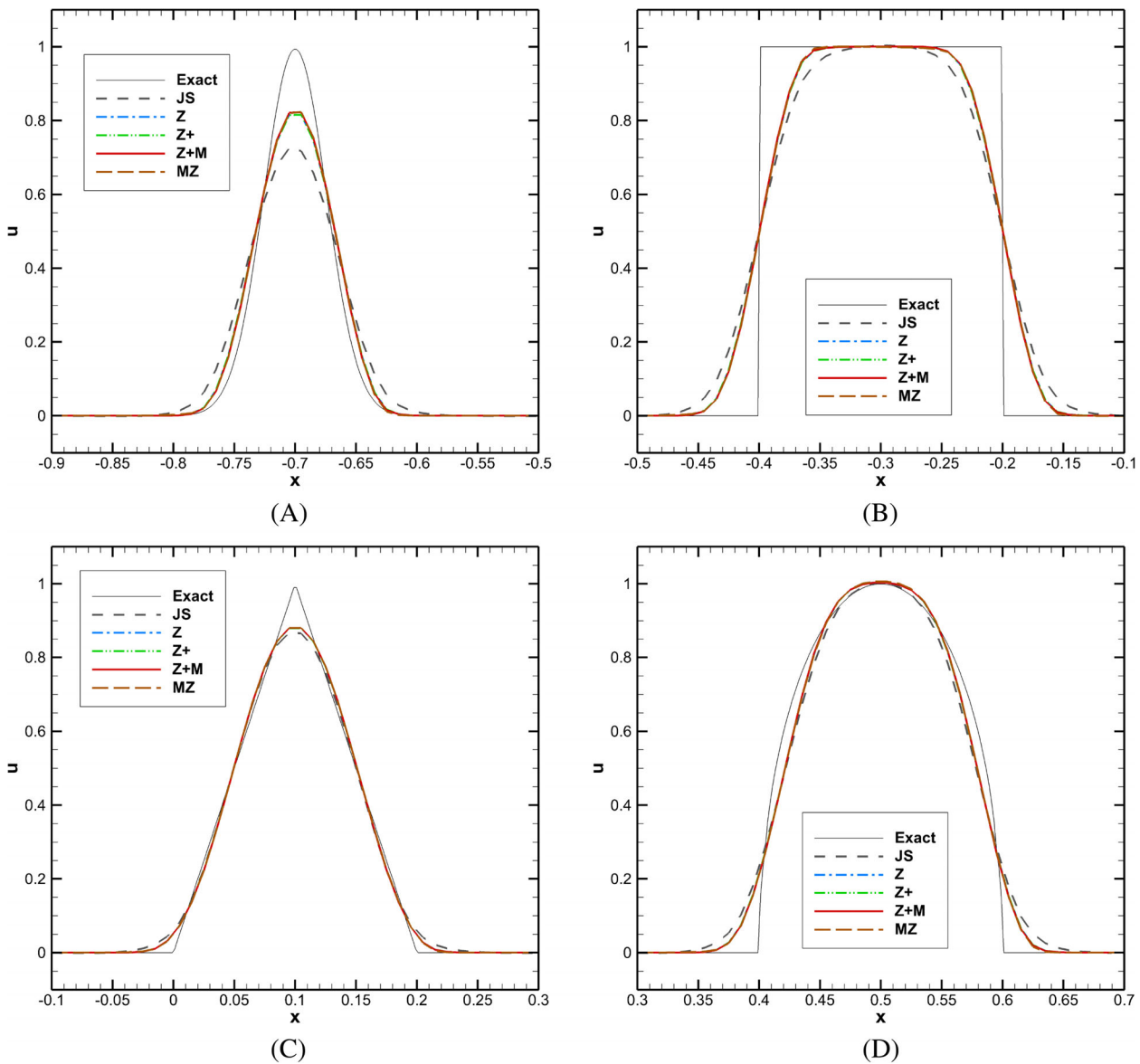
FIGURE 2 Results of the multi-wave problem (32) at $t = 6$ with $N = 200$ mesh cells. (A) Gauss wave zone; (B) square wave zone; (C) triangle wave zone; (D) semi-ellipse wave zone. [Colour figure can be viewed at wileyonlinelibrary.com]

4.3 | One-dimensional Euler equations

Consider the one-dimensional Euler equations

$$\mathbf{U}_t + \mathbf{F}(\mathbf{U})_x = 0 \tag{33}$$

with

$$\mathbf{U} = (\rho, \rho u, E)^T, \ \mathbf{F}(\mathbf{U}) = \left(\rho u, \rho u^2 + p, u(E + p)\right)^T.$$

Here, ρ, u, p and E are the density, velocity, pressure and total energy respectively, and the ideal gas equation of state is given by

$$p = (\gamma - 1)\left(E - \frac{1}{2}\rho u^2\right), \ \text{with} \ \gamma = 1.4.$$

4.3.1 | Lax problem

The first example is the Lax problem with the initial conditions[38]

$$(\rho, u, p) = \begin{cases} (0.445, 0.698, 3.528), & 0 \le x \le 0.5, \\ (0.500, 0.000, 0.571), & 0.5 < x \le 1. \end{cases}$$

The computational domain is $x \in [0, 1]$ with zero gradient boundary conditions applied on two ends and the final time is $t = 0.13$. The exact solution is computed by the exact Riemann solver.[39] Figure 3 shows the computed density profiles. For the shock wave and contact discontinuity, the WENO-MZ, WENO-Z+M and WENO-Z schemes have comparable
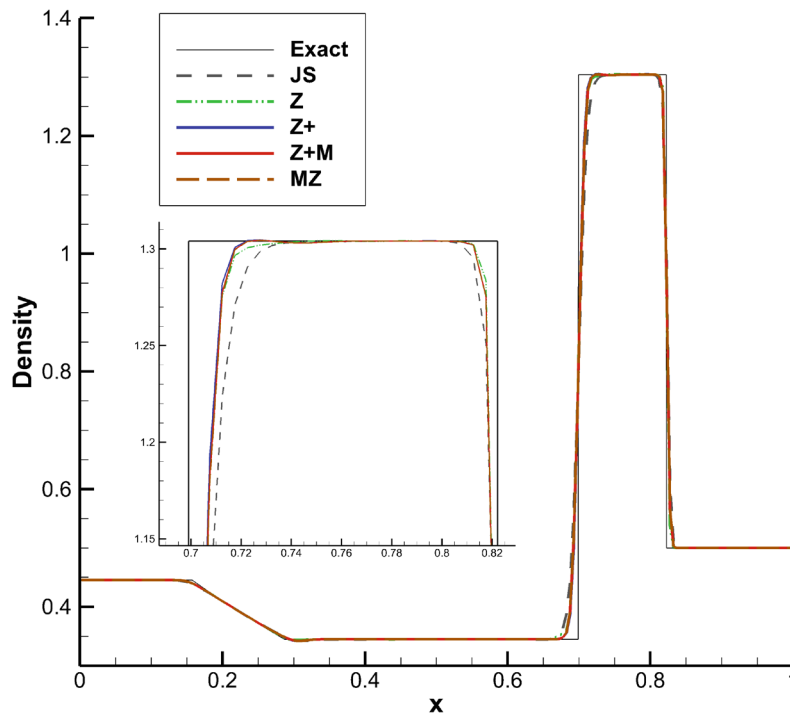
FIGURE 3 Density profiles with different schemes for the Lax problem at $t = 0.13$ with $N = 200$. [Colour figure can be viewed at wileyonlinelibrary.com]
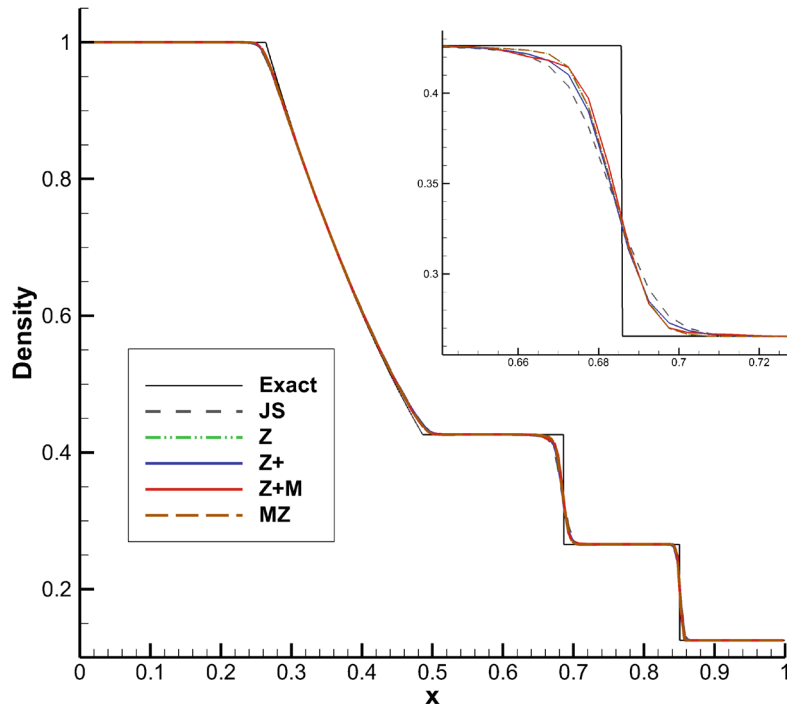
FIGURE 4 Numerical results of the Sod problem with $N = 200$ and the zoom-in view at $t = 0.2$. [Colour figure can be viewed at wileyonlinelibrary.com]

resolution which is higher than the WENO-Z+ schemes. All the WENO-Z types schemes have higher resolution than the WENO-JS scheme.

4.3.2 | Sod problem

The Sod's shock-tube test problem[40] is described with the initial conditions

$$(\rho, u, p) = \begin{cases} (1, 0, 1), & 0 \leq x \leq 0.5, \\ (0.125, 0, 0.1), & 0.5 < x \leq 1. \end{cases}$$

The computational domain is $x \in [0, 1]$ with zero gradient boundary conditions applied on two ends and the final time is $t = 0.2$. The solution contains a right moving shock wave, a right traveling contact wave and a left sonic rarefaction wave. The numerical results computed by five various schemes are shown in Figure 4. We can see that the results by the WENO-MZ and WENO-Z+M schemes are the best, followed by the WENO-Z, WENO-Z+, and WENO-JS schemes.

4.3.3 | Shock-entropy wave interaction problem

This problem describes a one dimensional moving shock interaction with a perturbed density field.[41] The initial conditions are

$$(\rho, u, p) = \begin{cases} \left(\frac{27}{7}, \frac{4\sqrt{35}}{9}, \frac{31}{3}\right), & -5 \leq x < -4, \\ (1 + \epsilon \sin(\kappa x), 0, 1), & -4 \leq x \leq 5. \end{cases}$$
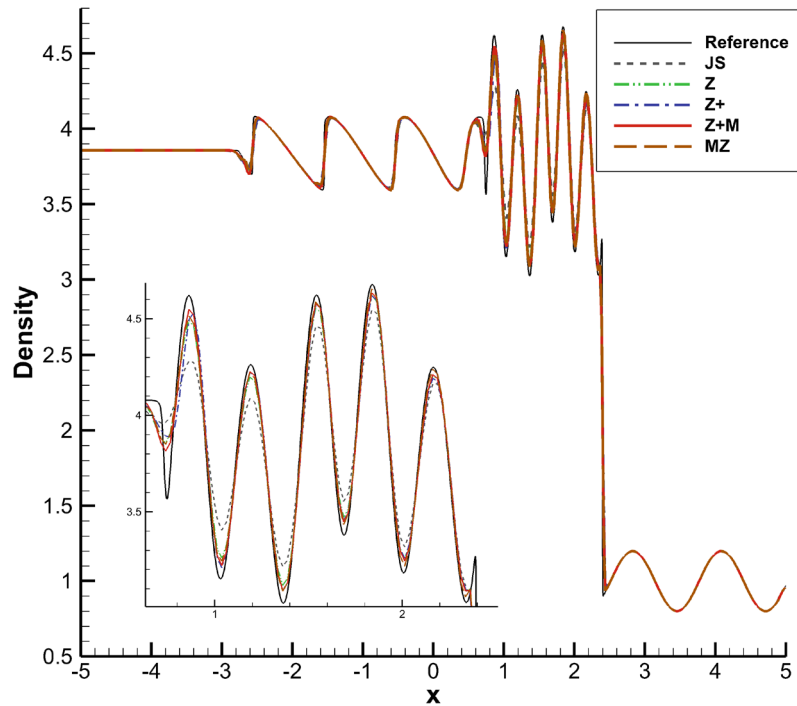
FIGURE 5 Density profiles for the shock-entropy wave interaction with $N = 400$ and the zoomed view at $t = 1.8$. [Colour figure can be viewed at wileyonlinelibrary.com]

Here, $\epsilon = 0.2$ and $\kappa = 5$ are the amplitude and wave number of the entropy wave respectively. The computation domain is $[-5, 5]$ with zero gradient boundary conditions applied on two ends and the final time is $t = 1.8$. When the shock interacts with the sinusoidal density perturbation, short wavelength high amplitude density waves are produced behind the shock. These waves are followed by a sequence of long wavelength low amplitude waves which steepen over time into N-shape waves. The reference solution is computed by the fifth-order WENO-JS5 scheme with $N = 4000$. The numerical results calculated by different schemes on a 400 points grid are shown in Figure 5. We see that the present WENO-Z scheme is slightly better than the WENO-Z+M, WENO-WENO-Z+ and WENO-Z schemes in the resolution of short wavelength large amplitude waves, and is much better than the WENO-JS scheme.

4.3.4 | Two interacting blast waves

This problem describes a two-blast-wave interaction problem.[42] The initial conditions are

$$(\rho, u, p) = \begin{cases} (1, 0, 1000), & 0 \leq x < 0.1, \\ (1, 0, 0.01), & 0.1 \leq x < 0.9, \\ (1, 0, 100), & 0.9 \leq x \leq 1. \end{cases}$$

with the reflective condition applied at both boundaries. The final time is $t = 0.038$ and the grid point number used is 400. The numerical results are shown in Figure 6. The reference solution is computed by the WENO-JS scheme with $N = 4000$ grid points. We see that the WENO-MZ scheme has higher resolution than the WENO-Z+M, WENO-Z+, WENO-Z, and WENO-JS schemes. This is particularly evident in the zoomed region.

4.4 | Two-dimensional Euler and Navier–Stokes equations

In the following, we test our scheme in four inviscid and one viscous 2D examples. We add numerical comparison with the fifth-order WENO-AO(5,3) scheme.[29]
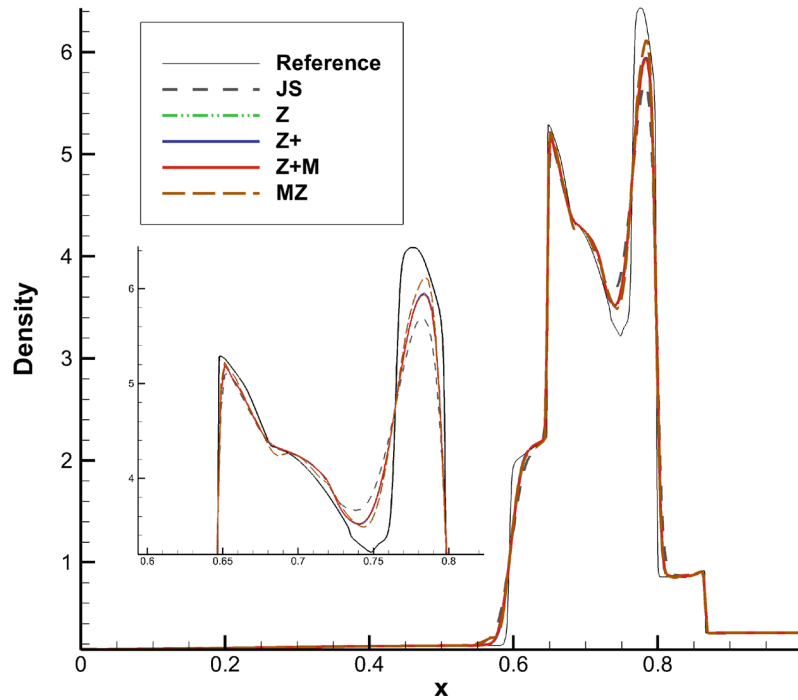
FIGURE 6 Density profiles of the two interacting blast wave problem with $N = 400$ and the zoom-in view at $t = 0.038$. [Colour figure can be viewed at wileyonlinelibrary.com]

4.4.1 | 2-D Riemann problem for gas dynamics

The initial conditions[43] are four constant states in four quadrants divided by lines $x = 0.8$ and $y = 0.8$ on the square $[0, 1] \times [0, 1]$:

$$(\rho, u, v, p) = \begin{cases} (1.5, 0.0, 0.0, 1.5), & 0.8 \leq x \leq 1.0, 0.8 \leq y \leq 1.0, \\ (0.5323, 1.206, 0.0, 0.3), & 0.0 \leq x < 0.8, 0.8 \leq y \leq 1.0, \\ (0.138, 1.206, 1.206, 0.029), & 0.0 \leq x < 0.8, 0.0 \leq y < 0.8, \\ (0.5323, 1.206, 0.0, 0.3), & 0.8 \leq x \leq 1.0, 0.0 \leq y < 0.8. \end{cases}$$

The boundary conditions are zero gradient boundary conditions.

Figure 7 shows the density contours with grid cells $N_x \times N_y = 400 \times 400$ at $t = 0.8$. It can be seen that the resolution of the vortical structures formed along the two slip lines from low to high is: WENO-JS < WENO-Z ≤ WENO-Z+ < WENO-Z+M ≤ WENO-AO(5,3) < WENO-MZ. In particular, the present WENO-MZ result has the highest resolution. Since the WENO-JS result is most diffusive and the WENO-Z result is similar to the WENO-Z+ one, to save space, we will not show the WENO-JS and WENO-Z results in the following 2D examples. Instead, we add comparison with the WENO-AO scheme (14).

Table 2 shows the timing results of the six compared WENO schemes for calculating the 2D Riemann problem. We see that the present WENO-MZ scheme has 9.1% extra computational cost relative to the WENO-Z scheme, the WENO-Z+M scheme has 6.1% extra cost, and the WENO-AO scheme has 20% extra cost.

4.4.2 | A Mach 3 wind tunnel with a step

This problem is set up with a Mach 3 flow in a wind tunnel with a forward-facing step.[42] The wind tunnel is 1 length unit wide and 3 length units long. The step is 0.2 length units high and is located 0.6 length units from the left-hand end of the tunnel. An inflow boundary condition is applied at the left end of the computational domain and an outflow
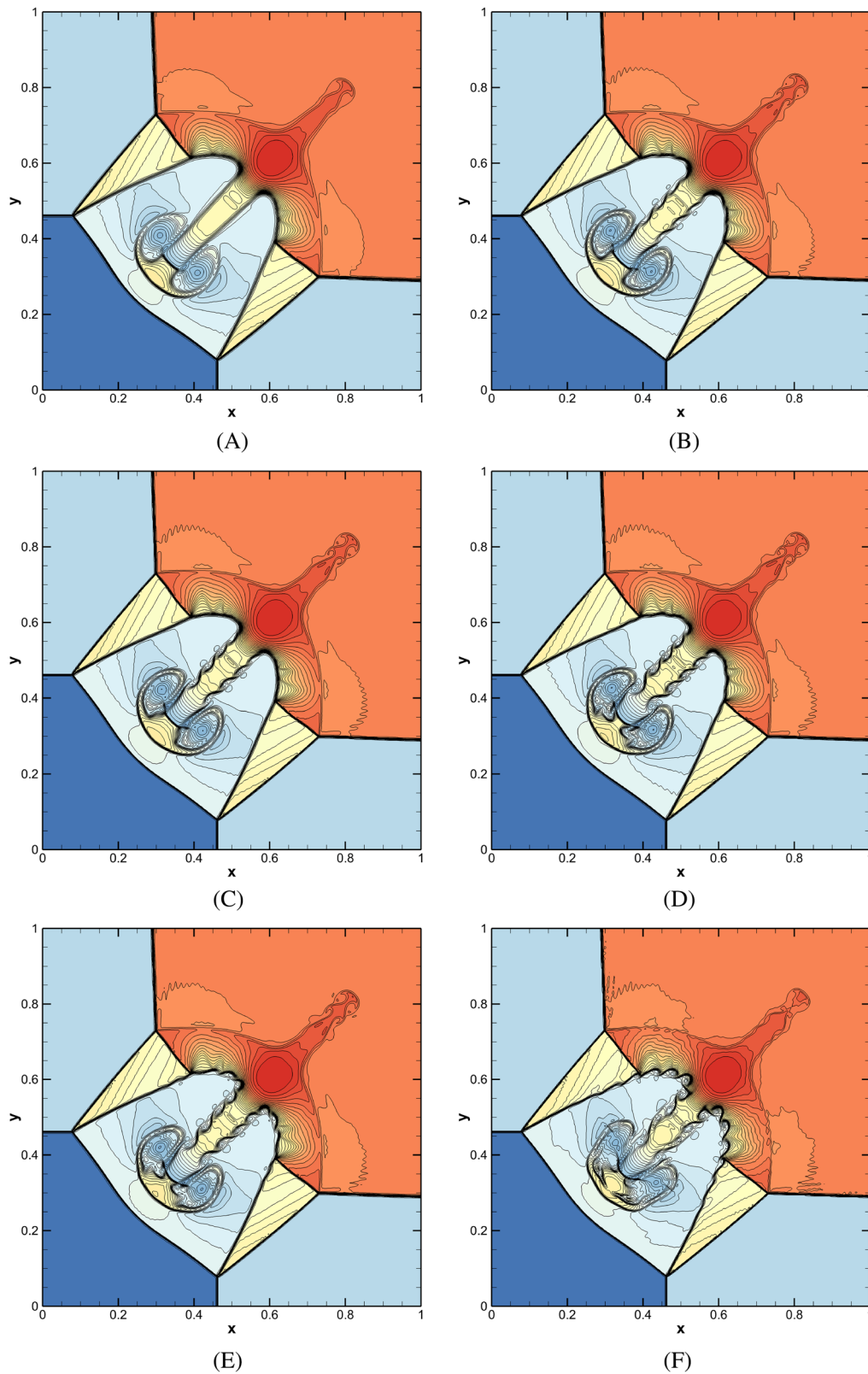
FIGURE 7 Density contours of two-dimensional Riemann problem at $t = 0.8$ with 400×400 grid cells. 40 equally spaced contours from 0.14 to 1.7. (A) WENO-JS; (B) WENO-Z; (C) WENO-Z+; (D) WENO-Z+M; (E) WENO-AO; (F) WENO-MZ. [Colour figure can be viewed at wileyonlinelibrary.com]

TABLE 2 CPU times in seconds taken by different schemes for simulating the 2D Riemann problem.

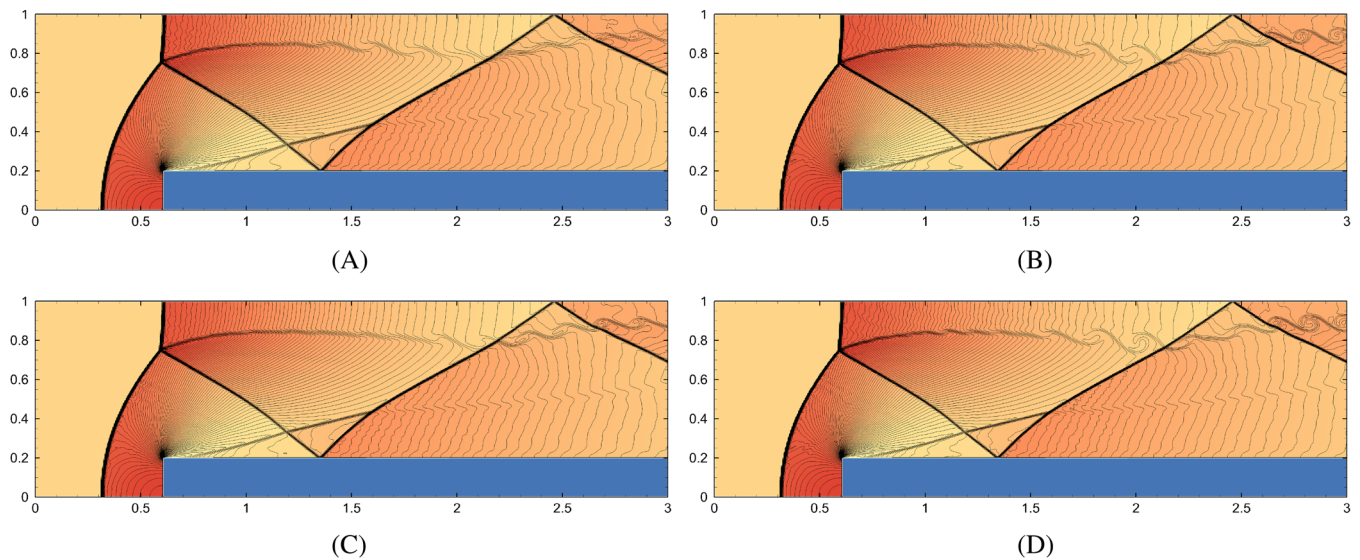| WENO-JS	WENO-Z	WENO-Z+	WENO-Z+M	WENO-MZ	WENO-AO
1193	1194	1212	1267	1303	1433

FIGURE 8 Density contours for the forward-facing step problem at $t = 4$ with 480×160 grid cells as in Reference 19. 90 equally spaced contours from 0.2568 to 6.607. (A)WENO-Z+; (B) WENO-Z+M; (C) WENO-AO; (D) WENO-MZ. [Colour figure can be viewed at wileyonlinelibrary.com]

boundary condition is applied at the right end. Along the walls of the tunnel we apply reflective boundary conditions. The initial condition is a $\gamma = 1.4$ gamma-law gas with $\rho = 1.4, u = 3.0, v = 0.0, p = 1.0$. Since the corner of the step is a singular point, we use the entropy correction technique[42,44] to cure the numerical boundary layer problem due to the singularity at the corner. Figure 8 shows comparison of computed density contours by the four schemes. Both the WENO-MZ and WENO-Z+M schemes have better resolution of the rolling vortices along the slip line issuing from the Mach stem than the WENO-AO and WENO-Z+ schemes. By careful comparison, the present WENO-MZ scheme is slightly better than the WENO-Z+M scheme.

4.4.3 | Double Mach reflection problem

This problem is widely used to test the performance of shock-capturing methods.[42] The computational domain is $[0, 4] \times [0, 1]$. Initially a right-moving Mach 10 shock wave is imposed and the shock front makes an angle of 60° with the x axis at $x_0 = 1/6$. The part from $x = 0$ to $x = 1/6$ along the bottom boundary is assigned the exact post-shock states and the region $x \in [1/6, 4]$ is a reflecting wall. The left boundary is assigned the initial post-shock states. For the right boundary at $x = 4$, normal gradients of all variables are set to zero. The top boundary is set to describe the exact motion of the Mach 10 shock.[16,42] The initial pre-shock and post-shock conditions are defined by

$$
(\rho, u, v, p) = \begin{cases} \left(8, 8.25\cos\left(\frac{\pi}{6}\right), -8.25\sin\left(\frac{\pi}{6}\right), 116.5\right), & x < x_0 + \frac{y}{\sqrt{3}}, \\ (1.4, 0.0, 0.0, 1.0), & x \geq x_0 + \frac{y}{\sqrt{3}}. \end{cases}
$$

The final time is $t = 0.2$. The grid of resolution used is 960×240 grid cells for all the schemes.

The numerical density contours obtained with different schemes are shown in Figure 9. The rolling-up vortices emanating from the slip line in the zone of $2.2 \leq x \leq 2.8$ can reflect the resolution capability of a numerical scheme. The earlier the beginning position of the rolling-up vortices, the higher the numerical resolution is. We can see that the sequence
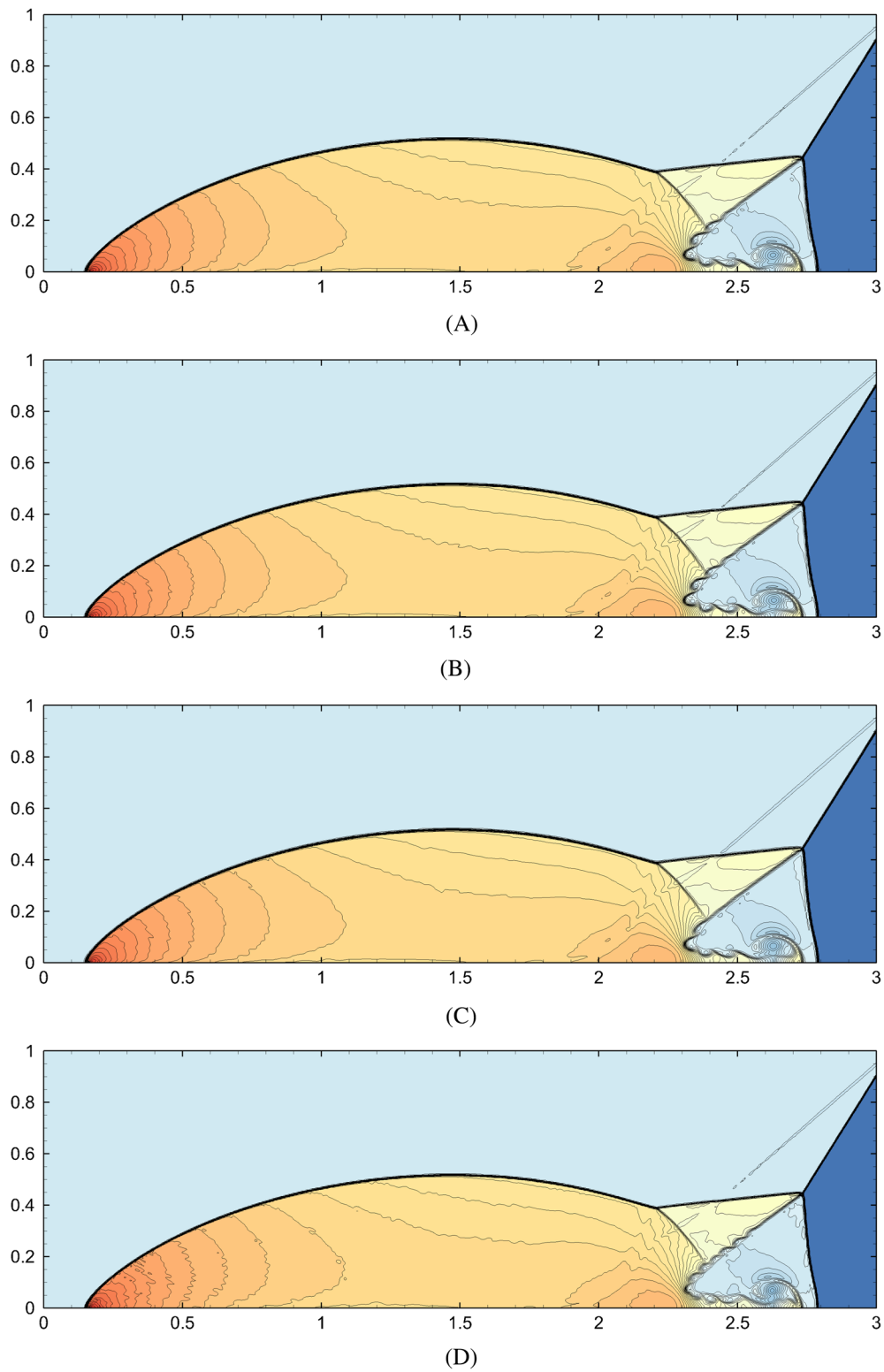
FIGURE 9 Density contours of double Mach problem at $t = 0.2$ with 960×240 grid cells and CFL = 0.5. 50 equally spaced contours from 2 to 22. (A) WENO-Z+; (B) WENO-Z+M; (C) WENO-AO; (D) WENO-MZ. [Colour figure can be viewed at wileyonlinelibrary.com]

of resolution from low to high is: WENO-AO < WENO-Z+ < WENO-Z+M < WENO-MZ. We note that for this example the WENO-AO(5,3) scheme has lower resolution compared to the WENO-Z+ scheme, which is contrary to the result for other 2D examples. Again, wee that the present WENO-MZ scheme has better resolution of the fine flow structures near the Mach stem than the other schemes.

4.4.4 | Rayleigh–Taylor instability

This problem describes the interface instability between two fluids with different densities when an acceleration is directed from the heavy fluid to the light one, and it is often used to test the numerical dissipation of a high order scheme.[45] The computational domain is $[0, 0.25] \times [0, 1]$. The top and bottom boundaries are set up as $(\rho, u, v, p) = (1, 0, 0, 2.5)$ and $(\rho, u, v, p) = (2, 0, 0, 1)$, respectively. Reflective boundary conditions are set for the left and right boundaries. The gravitational effect is introduced by adding ρ and ρv to the right hand side of the y-momentum and the energy equations, respectively. The ratio of specific heats is $\gamma = 5/3$. The initial conditions are given by

$$(\rho, u, v, p) = \begin{cases} (2, 0, -0.025\sqrt{\gamma p/\rho}\cos(8\pi x), 2y + 1), & \text{if } 0.0 \le y < 0.5, \\ (1, 0, -0.025\sqrt{\gamma p/\rho}\cos(8\pi x), y + 1.5), & \text{if } 0.5 \le y < 1.0. \end{cases}$$

The final simulation time is $t = 1.95$.

Figure 10 shows the results by the compared four schemes on the 240×960 resolution at $t = 1.95$. As in the literature, a more dissipative scheme is more likely to preserve the symmetry of the solution. A careful comparison about the vortical structures in the spike head shows that present WENO-MZ scheme has the highest resolution, followed by the WENO-Z+M, WENO-AO and WENO-Z+ schemes.

4.4.5 | Two-dimensional viscous shock-shear layer interactions

We also apply the present scheme to numerical solution of two-dimensional Navier–Stokes equations. We consider the shock-shear layer interaction problem, which can be used to check the resolution of a numerical scheme. The setup
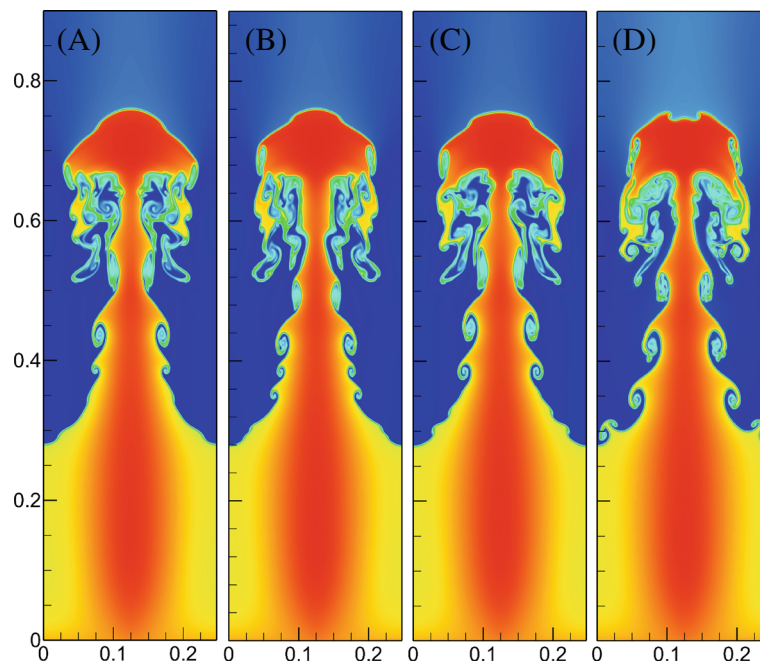

FIGURE 10 Density contours of Rayleigh–Taylor instability (from blue = 0.85 to red = 2.25) at $t = 1.95$ with 240×960 cells. (A) WENO-Z+; (B) WENO-Z+M; (C) WENO-AO; (D) WENO-MZ. [Colour figure can be viewed at wileyonlinelibrary.com]

and detailed description of this problem can be found in References 46 and 47 noting that slip-wall conditions are assumed at the bottom boundary to avoid any boundary-layer formation and subsequent complexities arising from the shock/boundary layer interaction. And the governing equations with an assumed constant physical viscosity are given in detail in Reference 48 and thus we will not repeat them here. A sixth-order central difference scheme is used to discretize the viscous terms. The simulation is carried on a uniform 251×51 grid as in Reference 19 with CFL = 0.5. The final time is $t = 120$. Figure 11 shows the density contours computed with four WENO schemes. Figure 12 shows the density profiles at $y = 0$ line computed with the four WENO schemes. The reference solution is computed by the WENO-Z scheme with 1251×251 grid points as in Reference 19. From Figure 12 we can see that the result of the WENO-MZ scheme is
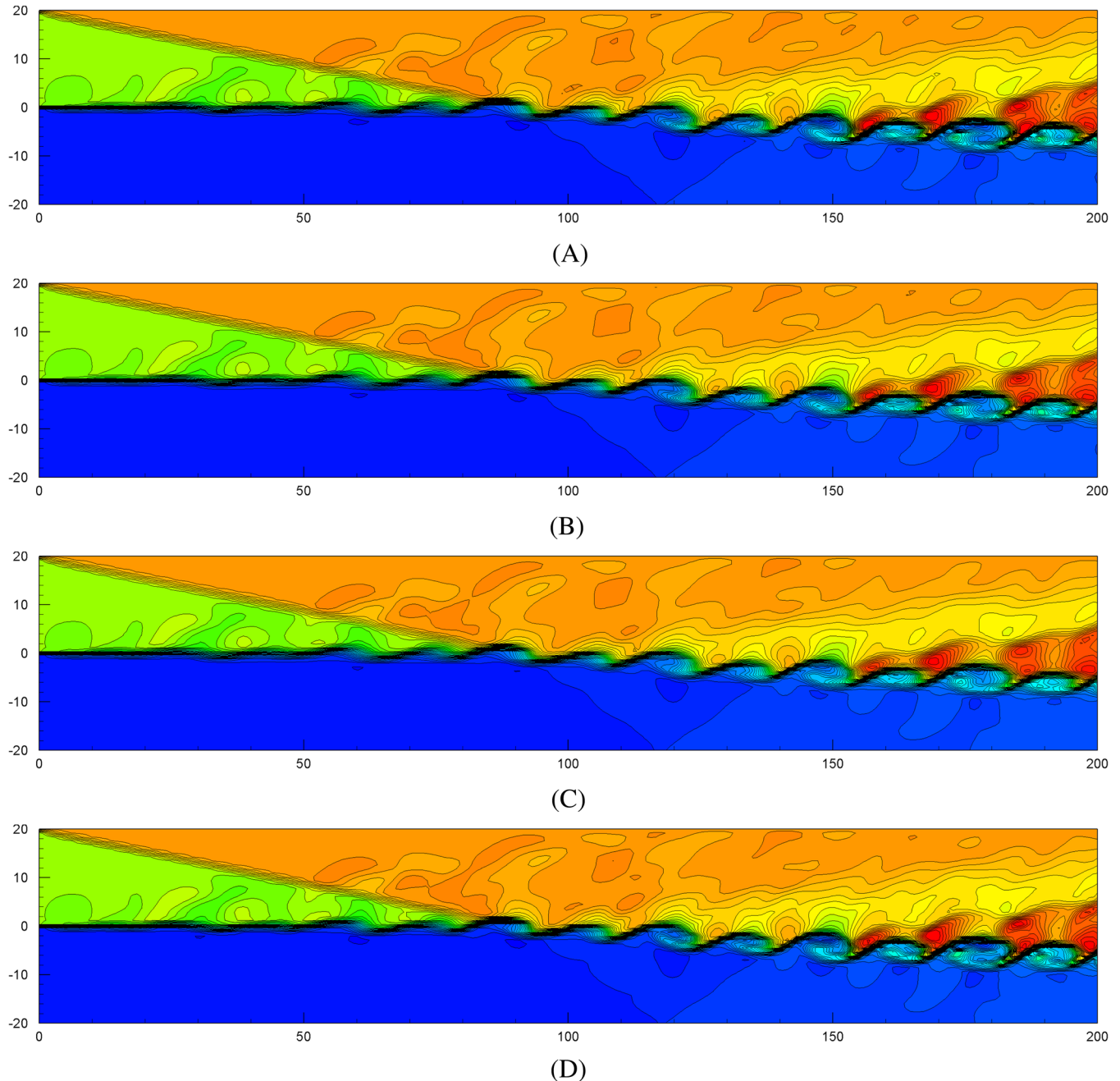

FIGURE 11 Density contours of shock-shear layer interaction problem at $t = 120$, CFL = 0.5, 251×51 grid points. 40 equally spaced contours from minimum to maximum. (A) WENO-Z+; (B) WENO-Z+M; (C) WENO-AO; (D) WENO-MZ. [Colour figure can be viewed at wileyonlinelibrary.com]
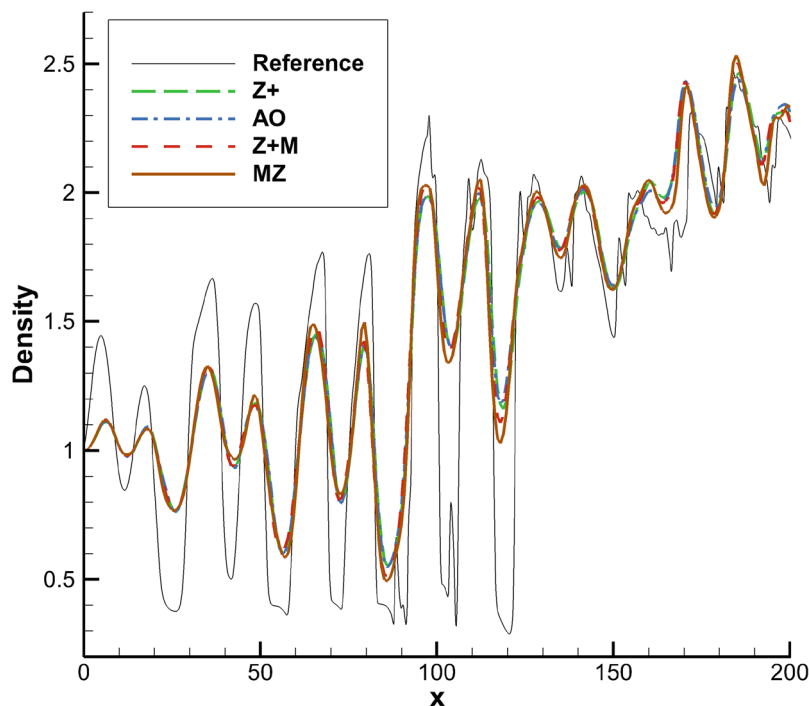
FIGURE 12 Density profiles of shock-shear layer interaction problem at $t = 120$, CFL $= 0.5$, 251×51 grid points. [Colour figure can be viewed at wileyonlinelibrary.com]

more close to the reference solution than the comparable WENO-Z+M scheme, while the WENO-AO and WENO-Z+ schemes are comparable and more away from the reference solution.

5 | CONCLUSIONS

A modified fifth-order WENO-Z (called WENO-MZ) scheme is presented. The non-normalized nonlinear weights of this scheme is inspired by those of the reformulated fifth-order adaptive order (AO) WENO scheme. By rewriting the original WENO-AO scheme as the conventional WENO combination form, we found that the non-normalized weights of the rewritten WENO-AO scheme have three terms, two of which are similar to those in the original WENO-Z scheme, and the third term is similar to the new term in the WENO-Z+ and WENO-Z+M schemes. In our modification, the fixed scaling factor in the non-normalized weights of the rewritten WENO-AO scheme is replaced by an adaptive one in order to recover quickly the underlying linear scheme better in smooth regions of the solution, and the third term is altered in order to reduce computational cost and account for substencil dependence. Numerical tests in typical 1D and 2D problems including Euler and Navier–Stokes systems demonstrated that the present WENO-MZ scheme can achieve evidently higher resolution compared with the fifth-order WENO-Z+ and WENO-Z+M schemes, while the computational cost per step is only a bit more than that of the WENO-Z+M scheme.

AUTHOR CONTRIBUTIONS
Yize Wang: Methodology; software; validation; visualization; writing – original draft; writing – review and editing. **Kunlei Zhao**: Methodology; software; validation; writing – review and editing. **Li Yuan**: Conceptualization; validation, writing – review and editing.

CONFLICT OF INTEREST STATEMENT

The authors declare no potential conflict of interests.

DATA AVAILABILITY STATEMENT

The data that support the findings of this study are available from the corresponding author upon reasonable request.

ORCID

Li Yuan 🟢 https://orcid.org/0000-0003-1397-9089

REFERENCES

1. Harten A, Engquist B, Osher S, Chakravarthy S. Uniformly high order essentially non-oscillatory schemes, III. *J Comput Phys*. 1987;71:231-303. doi:10.1016/0021-9991(87)90031-3

2. Liu XD, Osher S, Chan T. Weighted essentially non-oscillatory schemes. *J Comput Phys*. 1994;115:200-212. doi:10.1006/jcph.1994.1187

3. Jiang GS, Shu CW. Efficient implementation of weighted ENO schemes. *J Comput Phys*. 1996;126:202-228. doi:10.1006/jcph.1996.0130

4. Balsara D, Shu CW. Monotonicity prserving ENO schemes with increasingly high-order of accuracy. *J Comput Phys*. 2000;160:405-452. doi:10.1006/jcph.2000.6443

5. Henrick AK, Aslam TD, Powers JM. Mapped weighted essentially non-oscillatory schemes: achieving optimal order near critical points. *J Comput Phys*. 2005;207(2):542-567. doi:10.1016/j.jcp.2005.01.023

6. Feng H, Hu FX, Wang R. A new mapped weighted essentially non-oscillatory scheme. *J Sci Comput*. 2012;51(2):449-473. doi:10.1007/s10915-011-9518-y

7. Feng H, Huang C, Wang R. An improved mapped weighted essentially non-oscillatory scheme. *Appl Math Comput*. 2014;232:453-468. doi:10.1016/j.amc.2014.01.061

8. Vevek US, Zang B, New TH. Adaptive mapping for high order WENO methods. *J Comput Phys*. 2019;381:162-188. doi:10.1016/j.jcp.2018.12.034

9. Borges R, Carmona M, Costa B, Don WS. An improved weighted essentially non-oscillatory scheme for hyperbolic conservation laws. *J Comput Phys*. 2008;227(6):3191-3211. doi:10.1016/j.jcp.2007.11.038

10. Castro M, Costa B, Don WS. High order weighted essentially non-oscillatory WENO-Z schemes for hyperbolic conservation laws. *J Comput Phys*. 2011;230:1766-1792. doi:10.1007/s10915-014-9886-1

11. Jia FL, Gao Z, Don WS. A spectral study on the dissipation and dispersion of the WENO schemes. *J Sci Comput*. 2015;63(1):49-77. doi:10.1016/j.jcp.2010.11.028

12. Kim CH, Ha Y, Yoon J. Modified non-linear weights for fifth-order weighted essentially non-oscillatory schemes. *J Sci Comput*. 2016;67(1):299-323. doi:10.1007/s10915-015-0079-3

13. Zeng FJ, Shen YQ, Liu SP. A perturbational weighted essentially non-oscillatory scheme. *Comput Fluids*. 2018;172:196-208. doi:10.1016/j.compfluid.2018.07.003

14. Zhu J, Shu CW. A new type of multi-resolution WENO scheme with increasingly higher order of accuracy. *J Comput Phys*. 2018;375:659-683. doi:10.1016/j.jcp.2018.09.003

15. Hu XY, Wang Q, Adams NA. An adaptive central-upwind weighted essentially non-oscillatory scheme. *J Comput Phys*. 2010;229(23):8952-8965. doi:10.1016/j.jcp.2010.08.019

16. Hu FX. The 6th-order weighted ENO schemes for hyperbolic conservation laws. *Comput Fluids*. 2018;174:34-45. doi:10.1016/j.compfluid.2018.07.008

17. Wang YH, Du YL, Zhao KL, Yuan L. A new 6th-order WENO scheme with modified stencils. *Comput Fluids*. 2020;208:104625. doi:10.1016/j.compfluid.2020.104625

18. Acker F, Borges R, Costa B. An improved WENO-Z scheme. *J Comput Phys*. 2016;313:726-753. doi:10.1016/j.jcp.2016.01.038

19. Luo X, Wu SP. An improved WENO-Z+ scheme for solving hyperbolic conservation laws. *J Comput Phys*. 2021;445:110608. doi:10.1016/j.jcp.2021.110608

20. Don WS, Li R, Wang BS, Wang Y. A novel and robust scale-invariant WENO scheme for hyperbolic conservation laws. *J Comput Phys*. 2022;448:110724. doi:10.1016/j.jcp.2021.110724

21. Levy D, Puppo G, Russo G. Compact central WENO schemes for multidimensional conservation laws. *SIAM J Sci Comput*. 2000;22(2):656-672. doi:10.1137/S1064827599359461

22. Levy D, Puppo G, Russo G. A fourth-order central WENO scheme for multidimensional hyperbolic systems of conservation laws. *J Sci Comput*. 2002;24:480-506. doi:10.1137/S1064827501385852

23. Capdeville G. A central WENO scheme for solving hyperbolic conservation laws on non-uniform meshes. *J Comput Phys*. 2008;227:2977-3014. doi:10.1016/j.jcp.2007.11.029

24. Cravero I, Semplice M. On the accuracy of WENO and CWENO reconstructions of third order on nonuniform meshes. *J Sci Comput*. 2016;67:1219-1246. doi:10.1007/s10915-015-0123-3

25. Cravero I, Puppo G, Semplice M, Visconti G. CWENO: uniformly accurate reconstructions for balance laws. *Math Comput*. 2018;87:1689-1719. doi:10.1090/mcom/3273

26. Zhu J, Qiu JX. A new fifth order finite difference WENO scheme for solving hyperbolic conservation laws. *J Comput Phys*. 2016;318:110-121. doi:10.1016/j.jcp.2016.05.010

27. Hu C, Shu CW. Weighted essentially non-oscillatory schemes on triangular meshes. *J Comput Phys*. 1999;150:97-127. doi:10.1006/jcph.1998.6165

28. Shi J, Hu C, Shu CW. A technique of treating negative weights in WENO schemes. *J Comput Phys*. 2002;175:108-127. doi:10.1006/jcph.2001.6892

29. Balsara DS, Garain SK, Shu CW. An efficient class of WENO schemes with adaptive order. *J Comput Phys*. 2016;326:780-804. doi:10.1016/j.jcp.2016.09.009

30. Balsara DS, Garain S, Florinski V, Boscheri W. An efficient class of WENO schemes with adaptive order for unstructured meshes. *J Comput Phys*. 2020;404:109062. doi:10.1016/j.jcp.2019.109062

31. Shu CW, Osher S. Efficient implementation of essentially non-oscillatory shock-capturing schemes. *J Comput Phys*. 1988;77:439-471. doi:10.1016/0021-9991(88)90177-5

32. Hu FX. A note on WENO-Z scheme. *Appl Math Comput*. 2021;396:125886. doi:10.1016/j.amc.2020.125886

33. Zhao KL. *Several Modified Weighted Essentially Non-oscillatory Schemes and a Modified Hybrid Strategy*. PhD Thesis. University of Chinese Academy of Sciences; 2021.

34. Deng XG, Zhang HX. Developing high-order weighted compact nonlinear schemes. *J Comput Phys*. 2000;165(1):22-44. doi:10.1006/jcph.2000.6594

35. Fan P, Shen YQ, Tian BL, Yang C. A new smoothness indicator for improving the weighted essentially non-oscillatory scheme. *J Comput Phys*. 2014;269:329-354. doi:10.1016/j.jcp.2014.03.032

36. Shu CW. Essentially non-oscillatory and weighted essentially non-oscillatory schemes for hyperbolic conservation laws. Technical report NASA/CR-97-206253 (ICASE Report No. 97-65). Institute for Computer Applications in Science and Engineering, NASA Langley Research Center; 1997.

37. Jiang GS, Wu CC. A high-order WENO finite difference scheme for the equations of ideal magnetohydrodynamics. *J Comput Phys*. 1999;150:561-594. doi:10.1006/jcph.1999.6207

38. Lax PD. Weak solutions of nonlinear hyperbolic equations and their numerical computation. *Commun Pure Appl Math*. 1954;7:159-193.

39. Toro EF. *Rieman Solvers and Numerical Methods for Fluid Dynamics: A Pratical Introduction*. 3rd ed. Spring; 2009.

40. Sod G. A survey of several finite difference methods for systems of nonlinear hyperbolic conservation laws. *J Comput Phys*. 1978;27:1-31. doi:10.1016/0021-9991(78)90023-2

41. Shu CW, Osher S. Efficient implementation of essentially non-oscillatory shock-capturing schemes, II. *J Comput Phys*. 1989;83:32-78. doi:10.1016/0021-9991(89)90222-2

42. Woodward PR, Colella P. The numerical simulation of two-dimensional fluid flow with strong shocks. *J Comput Phys*. 1984;54(1):115-173. doi:10.1016/0021-9991(84)90142-6

43. Schulz-Rinne CW, Collins JP, Glaz HM. Numerical solution of the Riemann problem for two-dimensional gas dynamics. *SIAM J Sci Comput*. 1993;14(6):1394-1414. doi:10.3929/ETHZ-A-004283302

44. Donat R, Marquina A. Capturing shock reflections: an improved flux formula. *J Comput Phys*. 1996;125(1):42-58. doi:10.1006/jcph.1996.0078

45. Young YN, Tufo H, Dubey A, Rosner R. On the miscible Rayleigh-Taylor instability: two and three dimensions. *J Fluid Mech*. 2001;447:377-408. doi:10.1017/S0022112001005870

46. Yee HC, Sandham ND, Djomehri MJ. Low-dissipative high-order shock capturing methods using characteristic-based filters. *J Comput Phys*. 1999;150:199-238. doi:10.1006/jcph.1998.6177

47. Chaudhuir A, Hadjadj A, Chinnayya A, Palerm S. Numerical study of compressible mixing layers using high-order WENO schemes. *J Sci Comput*. 2011;47:170-197. doi:10.1007/s10915-010-9429-3

48. Daru V, Tenaud C. Evaluation of TVD high resolution schemes for unsteady viscous shocked flows. *Comput Fluids*. 2001;30:89-113. doi:10.1016/S0045-7930(00)00006-2